Electrodeposition and Corrosion Protection Performance of Polypyrrole Composites on Aluminum

Mahmoud A. Hussein[*]*, Salih S. Al-Juaid, Bahaa M. Abu-Zied, Abou-Elhagag A. Hermas*[*]

Chemistry Department, Faculty of Science, King Abdulaziz University, Jeddah 21589, Saudi Arabia
[*]E-mail: mahussein74@yahoo.com, hagag_99@yahoo.com

Electrodeposition of PPy-sCNTs and PANI-NiLa nanocomposites have been formed on aluminum using cyclic voltammetry technique. The process has been carried out from aqueous solution of 0.4 M oxalic acid containing 0.2 M pyrrole as a monomer and additives of nanopatricle materials. Presence of sCNT and Ni_2LaO_4 (NiLa oxide) nanoparticles in the electrolyte increased the electrodeposition rate of the PPy, the NiLa nanoparticles increased the deposition largely within the first fifty cycle. SEM images indicated emerging of the nanoparticles materials in the polymer layer forming nanocomposites. The sCNTs increased the thermal stability of PPy while the NiLa oxide nanoparticles decreased this stability. Improvements in the adhesion and protection role of the PPy coating for Al substrate were obtained in presence of sCNT and PPy-NiLa particles. All prepared nanocomposites layers protected Al better than that of PPy layer in NaCl solution. The highest protection was obtained by PPy-NiLa nanocomposite coating. The role of nanoparticles in the PPy coating and protection of Al was discussed.

1. INTRODUCTION

Many scientists are looking at the moment how to improve the properties of excisiting materials in addition to design new once with novel properties which will be compatible with the nature of the modern life. Aluminum is an important category of materials; it has a wide range of industrial and technological applications. The presence of a thin, adherent and protective surface oxide film make the aluminum has corrosion resistance in most environments. But, aluminum and its alloys are reactive materials and are suspected to pitting corrosion in seawater [1, 2]. So that, corrosion of Al and its alloys, particularly in chloride-containing solutions, has an enormous economic impact.

Conducting polymers are an important class of polymers which are mainly considered as one of the main components for corrosion-resistant coatings (3-5). Polypyrrole (PPy) is a famous conductive polymer that has been widespread studied in the last few decades. Pure pyrrole (Py) monomer can be easily polymerized to form PPy through oxidation mechanism with high thermal stability and electrical conductivity. The polymerization process can be carried out chemically or electrochemically. The physical as well as morphological behaviors of the synthesized film are varied from method to another method. This subsequently depending on the method of preparation, kind of the substrate, doping anion, kind & purity of the solvent and the pH value for the reaction [6–8]. Many studies have explained that PPy coating can be used as an substitutional component to the normal method of chromate coating as well as corrosion inhibitors versus the corrosion of nonferrous and ferrous metals [9–14]. PPy as all conducting polymer systems have efficient corrosion protection when it is in the conducting form (oxidized and doped state). Whereas, it loses the protection in its reduced form of the film [15, 16].

According to Hülser and coworkers [17], the presence of Al_2O_3 on the Al surface inhibits the electron transfer process thus hindering the PPy deposition and, hence, the polymer formation and growth. The pretreatment of the metal strongly influence the PPy film coherence and adhesion to the substrate and also the film formation begins inside the pores of the oxide. Polypyrrole/sodium dodecylbenzene sulfonate were electropolymerised on the surface of Al alloy (AA 1100) to evaluate their performance in terms of corrosion protection of the alloy in chloride solutions [18]. The electrochemical synthesis of adherent and homogenous PPy films on Al and Al/Cu samples were successfully achieved, by Mert et al [19], from 0.1 M monomer containing oxalic acid medium and using cyclic voltammetry technique. Turhan et al [20] showed that the initial and end potential values during the electrochemical coating play an important role on the adhesion and corrosion performance of PPy films on Al alloy surface.

To increase the efficiency of conductive polymer as a protective coating on metals, several strategies have been used. Nanoparticles of different natures, such as ones prepared from carbon nanotubes, natural fibers, nanoclays (layered silicates) graphite and any other inorganic materials [21-25], are used as additives to promote barrier performance and the mechanical of polymers has been instituted. For example, TiO_2 [26, 27], ZrO_2 [28] and SiO_2 [29] particles have been combined with polypyrrole and/or polyaniline matrices. Zhu and Iroh [29] synthesised polyaniline using electrochemical method on an AA2024 aluminium alloy and in the presence of nanoparticles such as those particles. Nanocomposites in the form of polypyrrole/TiO_2 nanocomposite films displayed developed behavior compared with the original polypyrrole films. Such performance was due to the diminutive porosity of the polymer through filling by TiO_2 particles [30]. In our previous studies, presence of CNTs in the electrolyte promoted the electropolymerization process on the stainless steel surface and the fabricated layer outlined a promised protective action against corrosion [31, 32]. It was reported the passivation of the stainless steel has been supported easily in the presence of CNTs by indirect way. This is mainly attributed to catalytic polymer oxidation and oxygen reduction process. In this paper, corrosion protection of aluminum using well adherent nanocomposites based on polypyrrole containing nanoparticles of NiLa oxide and single wall carbon nanotubes will be studied.

2. EXPERIMENTAL WORKS

All chemical materials were used from analytical grades (Merck and Aldrich) and the solutions were prepared from doubly distilled. Pyrrole monomer was distilled before use, whereas the other chemicals were used as received without further purification. Electrochemical experiments were proceeded in a single chamber cell with three-electrode. The material of the working electrode is pure aluminum in the form of a rod machined into a cylindrical form embedded in epoxy resin leaving an open surface area of 1 cm^2. Before attempting the measurements it was pre-handled by mechanical polishing with emery papers of different grades up to 1000 grit, degreased with acetone, washed with bi-distilled water. Then, the electrode is immersed in a freshly prepared 1M NaOH solution for one minute to remove the surface oxide film and finally washed with bi-distilled water [33]. The counter electrod is platinum sheet while reference electrode is silver-silver chloride (Ag/AgCl, 3 M KCl), respectively. Square panels of Al, to electrodeposit polymer coating films on one side with area 9 cm^2, were specially prepared for the adhesion test. It is well known that, CNTs nanoparticles are hydrophobic in nature and very hard to be suspended in water. Thus and in order to simplify the suspension of CNTs in water and to form its hydrophilic phase as well. A mixture of sulfuric and nitric acids was introduced and acidic functional groups are formed on their surfaces through oxidation [32]. The Ni-La oxide (Ni$_2$LaO$_4$) nanoparticles were prepared using the same method as described before [34]. Electrochemical characterizations and electropolymerization were measured using a computerized Autolab PGSTAT 30 potentiostat/galvanostat with GPES software. The cyclic voltammetry method within potential range 0.6-1.4 V (Ag/AgCl) and a scan rate 50 mV s^{-1} was used for the electrodeposition of the conductive polymer at room temperature. To investigate the corrosion performance of the polymer-coated Al samples, open-circuit potential measurements versus time were used in corrosive acidic and chloride solutions. The deposited polymer layers were investigated using different techniques. Scanning electron microscopic investigation was performed by using FEI- Field Emission Scanning Electron Microscope (FE-SEM) Quanta FEG 450, Netherlands. The FT-IR investigation was measured by Thermo-Nicolet-6700 FTIR spectophotometer. The thermal analysis was done using TGA7 Perkin Elmer thermal analyzer system in air with a scan 10°C/min. The adhesion of coating PPy films to substrate is examined by stratifying and taking off pressure-sensitive tape over cuts in the film (ASTM D-3359 standard method).

3.RESULTS AND DISCUSSION

3.1 Electrodeposition

Figure 1 shows some selected cycles of cyclic voltammetry (CV) of PPy deposition on Al electrode from 0.4 M oxalic acid containing 0.2 M pyrrole. The electropolymerization was performed within potential range 0.6-1.4 V (Ag/AgCl). The first cycle indicates a sharp increase in the anodic current at about 0.65 V (Ag/AgCl) forming a large anodic oxidation peak of the monomer and thus polymer formation. The oxidation potential of the pyrrole shifted to more positive with the successive cycles due to the deposition of the polymer layers. The oxidation-reduction peaks of the polypyrrole are observed at 0.02/-0.468 V (Ag/AgCl) according to the reaction:

$$[PPy^{y+}(C_2O_4{}^{2-})_y]_n + 2nye \Leftrightarrow (PPy)_n + ny\,C_2O_4{}^{2-} \quad (1)$$
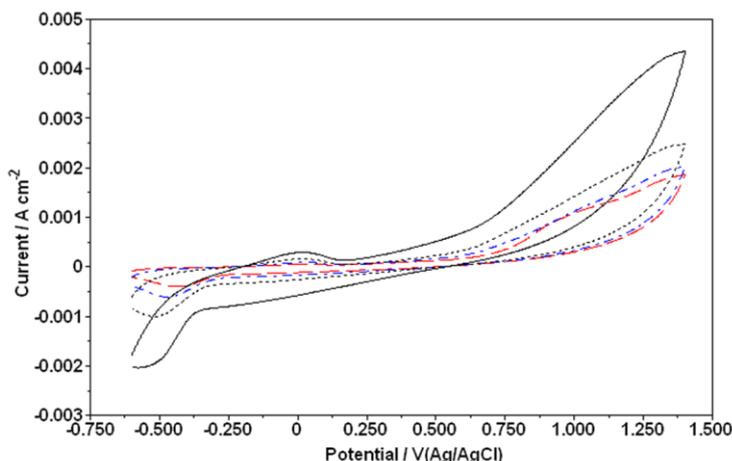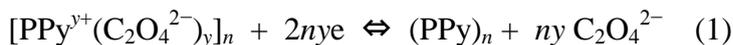
Figure 1. Selected successive cycles (no. 3, 10, 15, 25) of cyclic voltammetry (scan rate 50 mV s^{-1}) of PPy on Al from 0.4M oxalic acid containing 0.2M pyrrole at room temperature.

This redox process involves doping/depoing of oxalate ions. The large separation peaks of this couple system may be rlated to slow diffusion of oxalate ions. Similar cyclic voltamograms were obtained for electropolymerization of pyrrole on different electrode materials [35-37]. A macroscopically continuous brown-black film on the Al surface can be observed at the end of the experiment.

The presence of nanoparticles additives in the electrolyte solution was found to enhance the electropolymerization process. The electro-growth rate of the PPy is determined by considering the variation of the coulomb charge (Q) included in the oxidation peak of the CV as a function of the cycle number [38]. The charge of the pyrrole oxidation in each cycle was calculated by the mathematical integration of the anodic curve using GPES program.
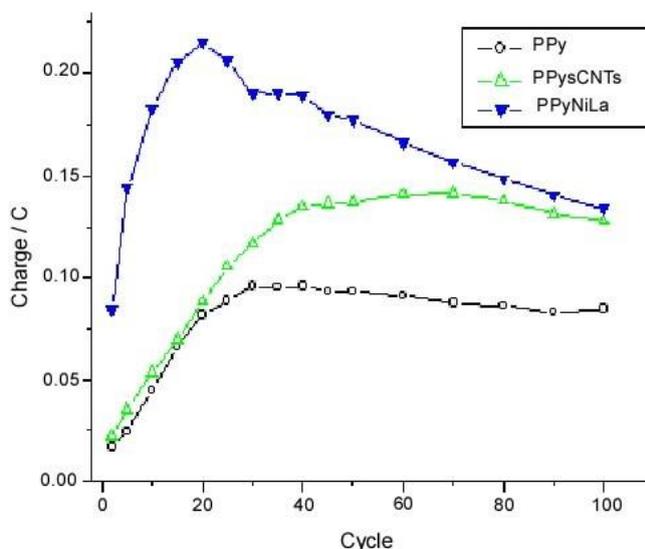
Figure 2. Electrodeposition rate of PPy and its nanocomposites on Al from 0.4M oxalic acid electrolyte solution containing monomer and nanoparticles at room temperature.

Figure 2 shows Q-cycle number relation for preparation of PPy and its nanocomposites on Al electrode. The growth rate of PPy deposition increases linearly with the cyclic number up to ~ 20 cycles after which the PPy decreases slightly or becomes stable growth. The slowdown of the PPy growth at higher cycles may be related to lower in the polymer conductivity with increasing in the thickness of the deposited layer. The existence of sCNTs in the electrolyte solution increased the rate of electropolymerization linearly up to 40 cycles, then slightly up to 80 cycles after then decreased slightly. The catalytic effect of the carbon nanotubes was observed before in electrodeposition of PPy [38] and other polymers [31, 32] on SS electrode surface. Presence of Ni-La oxide nanoparticles in the electrolyte solution highly increased the electrodeposition of PPy within the first 20 cycles then slowdown to a level of rate near to that contains the CNTs.

3.2 SEM examination and adhesion test
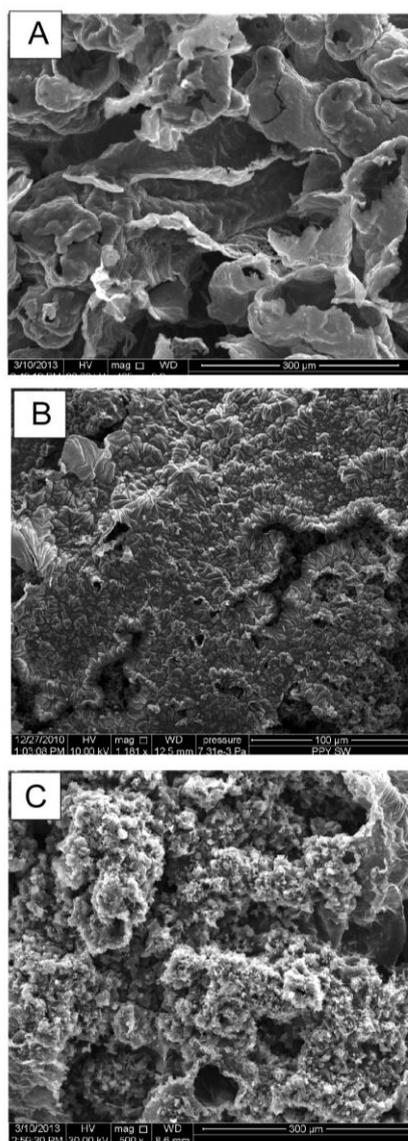
Figure 3. SEM micrographs at low magnification (x100) of PPy (A), PPy-sCNTs (B) and PPy-NiLa (C) after 30 cycles electrodeposition.
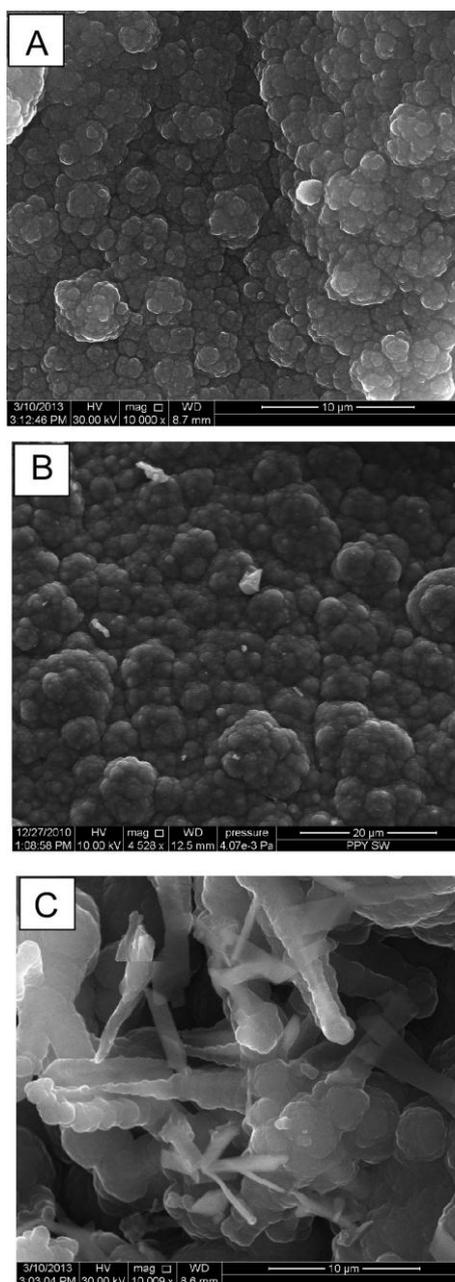
Figure 4. SEM high magnification micrographs at high magnification (x1500) of PPy (A), PPy-sCNTs (B) and PPy-NiLa (C) after 30 cycles electrodeposition.

A thick dark brown layer of the deposited PPy was observed after 100 cyclic voltammograms, while blackish layer deposited in case of PPy containing sCNTs, indicating of mixing of these nanoparticles with the polymer.

The SEM images at lower magnification (x100) of the deposited polymer layers are indicated in Fig.3, it is obvious that the presence of CNTs and NiLa nanoparticles make the grains of the PPy much finer. At high magnification (x15000) in Fig.4, image Fig.4 −A indicates globular characteristic morphology of the PPy and the layer becomes more condense in presence of sCNTs as in Fig.4-B. A noodles shape of the deposited polymer in presence of Ni-La oxide nanoparticles was observed as shown in Fig.4-C. After electrodeposition of the different coatings and drying for 48 hours in dry air at

25◦C, the adhesion test was carried out. The results clearly indicated that the adherence of the coating to the substrate increased in the order PPy < PPy-sCNT < PPy-NiLa.

3.3 Thermal analyses (TGA & DTA)

The thermal behavior of the neat PPy and its nanocomposites was estimated by TGA and DTA analyses at a heating rate of 10 °C/min in air flow (40 ml/min).
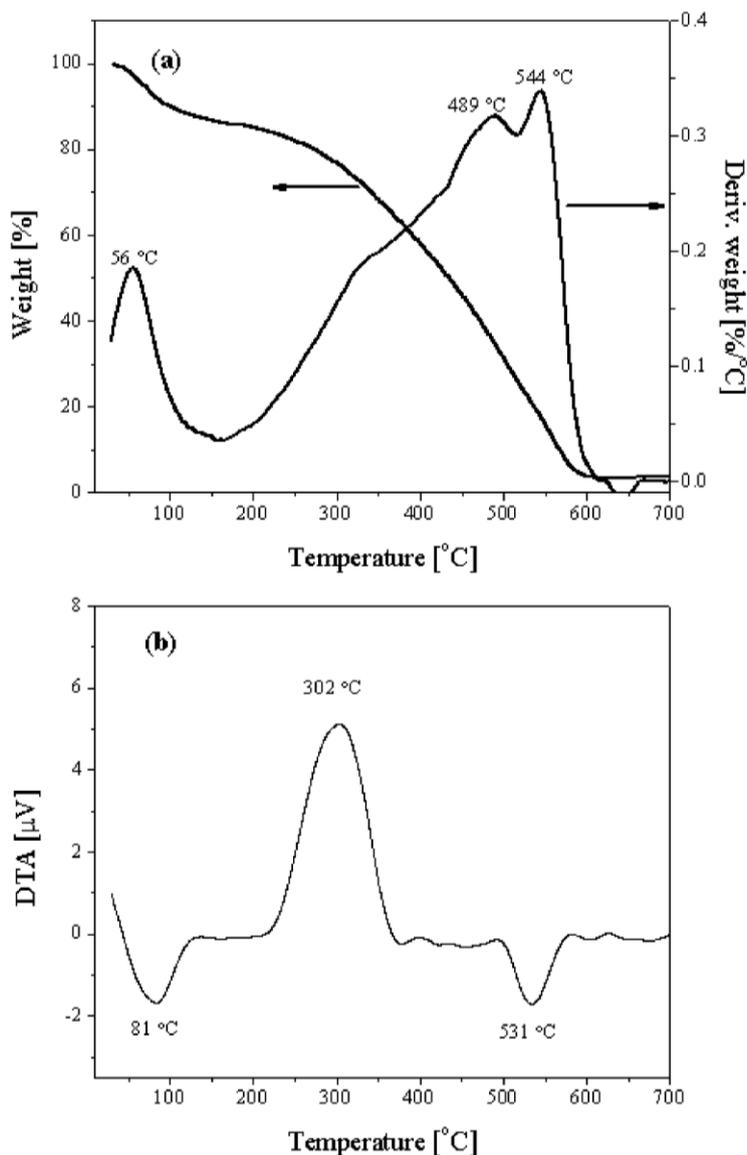
Figure 5. TGA (a) and DTA (b) thermograms obtained for the electrodeposited layer of PPy analyses at a heating rate of 10 °C/min in air flow (40 ml/min).

Fig. 5-a shows the TGA and DTG curves obtained for the neat PPy. Two main weight loss (WL) steps can be identified; the first one extends from ambient till around 165 °C, which is maximized at 56 °C and accompanied by a WL of 14 %. The second WL step is a little pit complicated and not like not a simple one; instead it is a composite step with two maxima at 489 and 544 °C (DTG

curve) which coincides to a total weight loss of 82.29 %. These two WL steps could be anticipated to the loss of moisture and the oxidative decomposition of PPy chains. In agreement, Mavinakuli et al. [39] reported two stages for the thermal decomposition of PPy, in air atmosphere, at 26 - 220 and 220 - 650 °C, which were ascribed to the elimination of moisture and solvent and the decomposition of PPy, respectively. Similar thermal behavior of polypyrrole was also reported by other authors [38-47]. Inspection of the DTA thermogram of nest PPy, Fig. 5-b, reveals the presence of two endothermic effects at 81 and 531°C and one exothermic effect at 302 °C.
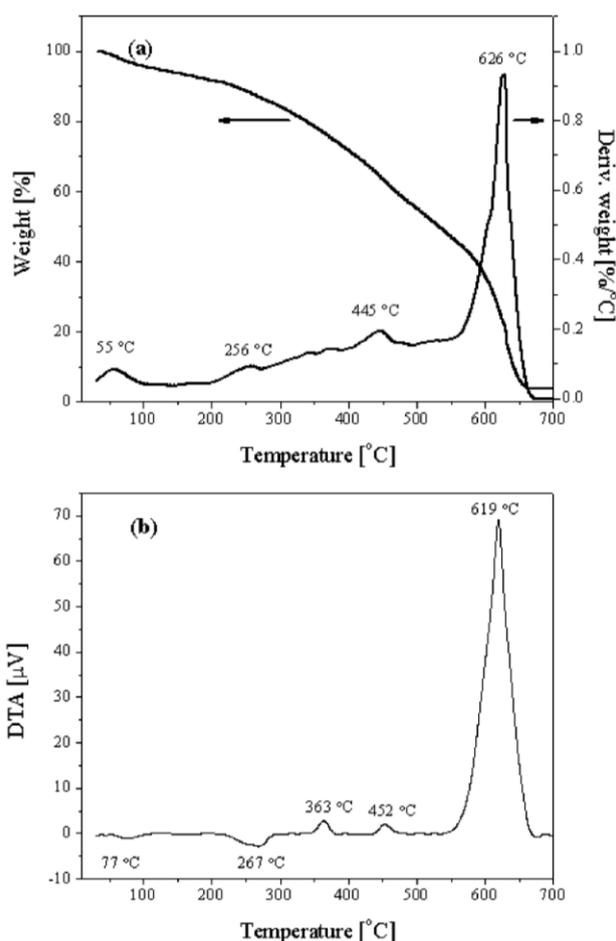
Figure 6. TGA (a) and DTA (b) thermograms obtained for the electrodeposited layer of PPy-sCNTs analyses at a heating rate of 10 °C/min in air flow (40 ml/min).

The endothermic effect at 81 °C could be related to the glass transition temperature (T_g) of PPy [39, 40]. It was shown that under nitrogen flow the DSC thermogram of pure PPy contains one more peak at 295.2 °C, which is attribute to the PPy melting point [39]. When the measurement is carried out in air flow, Abthagir and Saraswathi [41] reported a broad exothermic effect (250-700 °C) during the decomposition of PPy. From these literature data, it appears that within the temperature range of 250-700 °C two opposing thermal effects exist; (i) endothermic, which is due to the melting followed by the decomposition of PPy, and (ii) exothermic, which is attributed to the combustion of the evolved gases. From the detection of only one exothermic peak 205-375 °C under air flow, Fig. 5-b, it seems that the second effect predominates. Lapides et al. [44, 45] studied the thermal decomposition montmorillonite intercalated with organic molecules. They demonstrated that the evolution of organic

matter, started at around 250 °C, is accompanied by the formation of: (i) low temperature stable charcoal (LTSC), (ii) high temperature stable charcoal (HTSC-α) and (iii) high temperature stable charcoal (HTSC-β). Accordingly, it is plausible to relate the observed endothermic effect at 531°C, Fig.5-b, to the removal of the high temperature stable charcoals.
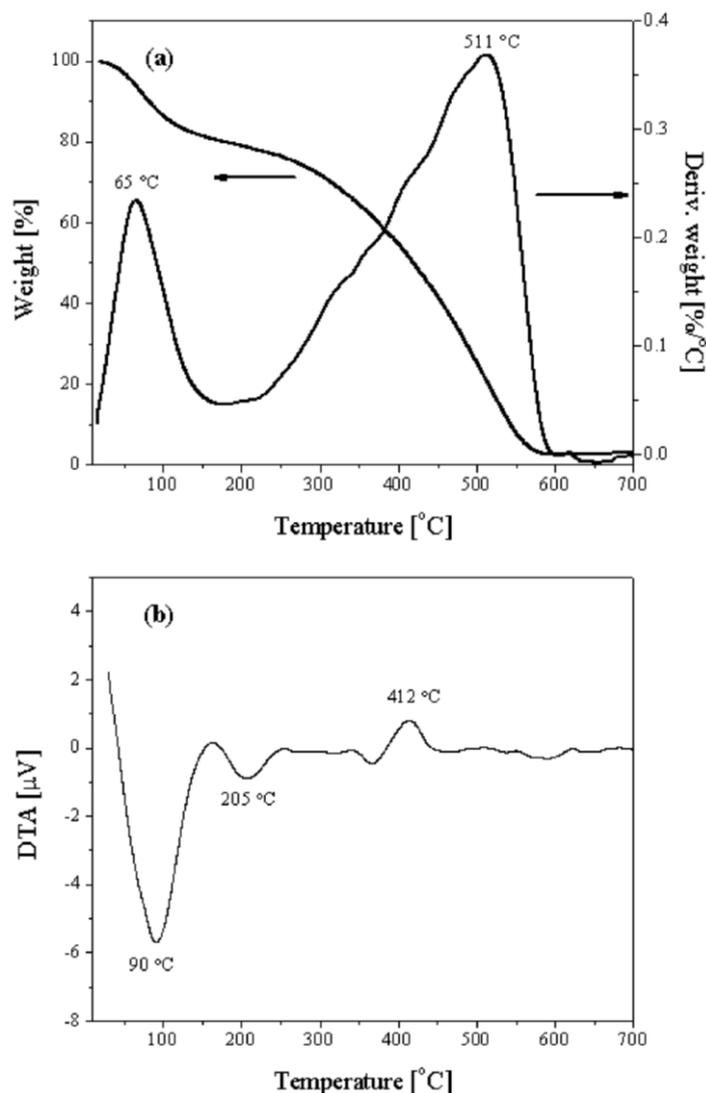
Figure 7. TGA (a) and DTA (b) thermograms obtained for the electrodeposited layer of PPy-NiLa analyses at a heating rate of 10 °C/min in air flow (40 ml/min).

The TGA thermogram of PPy-NiLa nanocomposite, Fig.6-a, also shows two WL steps, which are maximized at 65 and 511 °C. The relevant DTA curve of this nanocomposite, Fig. 6-b, exhibit an endothermic effect at 90 °C, due to the PPy glass transition, and another two effects at 205 °C (endothermic) and 412 °C (exothermic). The effect at 205 °C could be anticipated to the start of the PPy decomposition whereas the effect at 412 °C to the combustion of the evolved gases. The smaller magnitude of the exothermic effect at 412 °C, Fig. 6-b, compared to that at 302 °C, Fig. 5-b, could be attributed to the superposition of the evolved gases combustion (exothermic) and the charcoal elimination (endothermic).

Table 1. TGA data obtained for the neat PPy and its nanocomposites under air atmosphere.

Sample	T_{25} / °C	T_{50} / °C	T_{75} / °C	R_{675}/%
PPy	313	433	519	3.71
PPy-sCNTs	376	532	622	3.45
PPy-NiLa	262	418	501	2.85

T_{25}, T_{50}, T_{75} (the temperatures of 25, 50, and 75 % weight loss, respectively), and the solid residue left at 675 °C are the main criteria indicating the thermal stability of the nanocomposites. These data are listed in Table 1. It is evident from Table 1 that the presence of La_2NiO_4 in the PPy-composite matrices shifts the T_{25}, T_{50} and T_{75} towards lower values. In other words, the presence of La_2NiO_4 enhances the thermal decomposition of PPy. This finding goes parallel with our most recent work on the catalytic effect of La_2NiO_4 during the decomposition of epoxy-resin composites [46].

Fig. 7-a depicts the TGA and DTG curves obtained for PPy-sCNTs in air flow. A close inspection of this figure reveals the presence of an early WL step at 55 °C, which is amounted to 5.5 WL% and could be related to the dehydration of the composite. This step is followed by a gradual composite WL step having two maxima at 256 and 445 °C. This step is probably due to the PPy decomposition. Finally, one can observe a steep WL maximized at 626 °C, which is accompanied by a sharp exothermic effect at 619 °C in the relevant DTA curve (Fig. 7-b. This step could plausibly be ascribed to the elimination of sCNTs [38]. The values of T_{25}, T_{50} and T_{75} are 376, 532, and 622 °C, respectively, as given in Table 1. These values are much higher than the relevant ones of the neat PPy, which in turn suggests the enhancement effect of sCNTs on the thermal stability of PPy. The improved thermal stability in PPy/sCNTs nanocomposites systems relative to the neat PPy have been recently reported by other research groups [42, 43]. The increased thermal stability of PPy via the nanocomposite formation with other materials like SiC and Fe_2O_3 was also reported [39, 47]. In agreement with these literature data, the observed higher thermal of PPy-sCNTs suggests the existence of an interfacial interaction between sCNTs and the polymer shell.

3.4 Protection characteristic of the coatings in aggressive solutions

Immersion tests in acidic and chloride solutions and measuring of the open-circuit potential in time were used as effective corrosion behavior of the coated samples in this study. Figure 8 shows the potential-time behavior of the different coated Al samples in 0.5 M H_2SO_4 at room temperature. The uncoated Al electrode on immediate immersion exhibited an active dissolution behavior where it started with potential -0.79 V and changed rapidly to steady state potential -0.725 V. The PPy-Al sample started with nobler potential ~ 0.2 V and decreased gradually up to the steady potential of the bare Al after two hours of immersion. But, the PPy-sCNTs and PPy-NiLa nanocomposite coatings kept the Al electrode at steady potential about 220 mV more positive than that of the bare Al, indicating that

these coatings has better protection than of the neat PPy layer. The PPy-NiLa nanocomposite coating exhibited the longest stable positive potential.
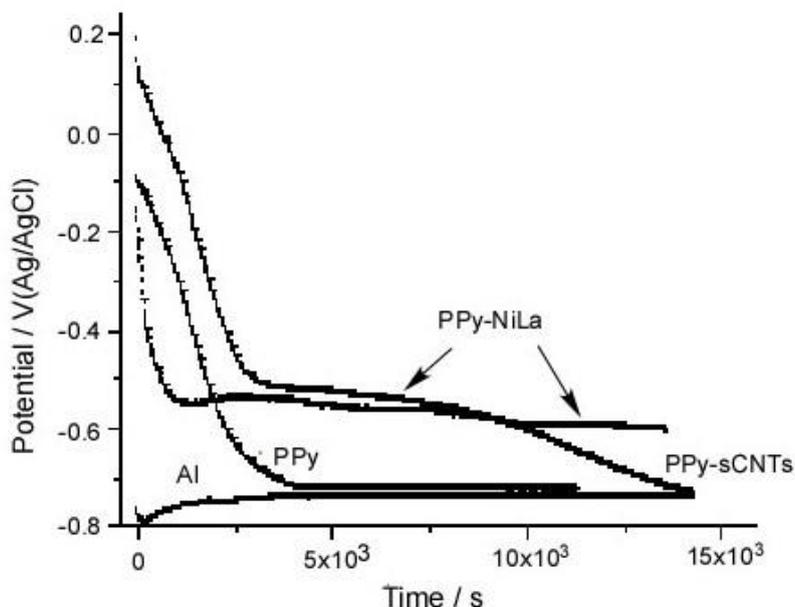
Figure 8. Potential-time relation of Al and different coated Al electrodes in 0.5M H_2SO_4 at room temperature.
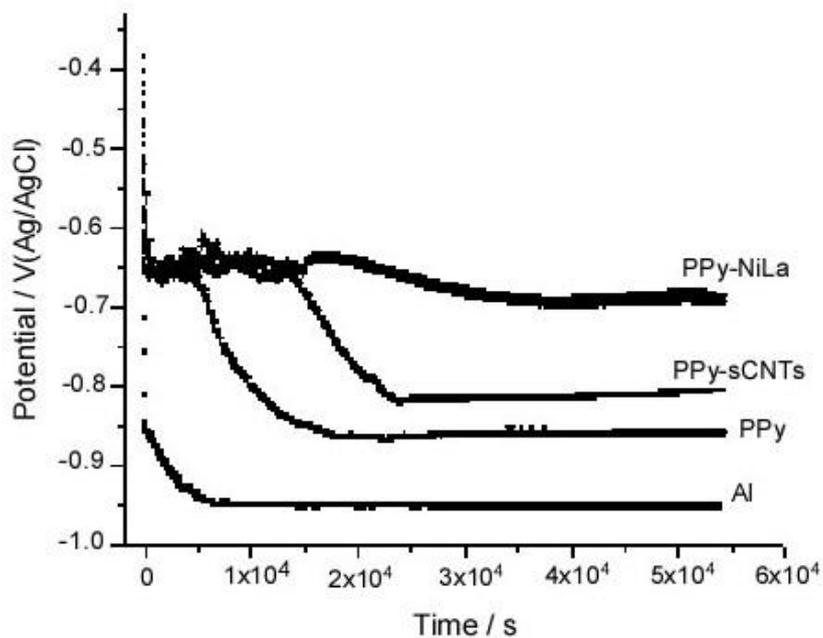
Figure 9. Potential-time relation of Al and different coated Al electrodes in 0.1M NaCl at room temperature.

The galvanic coupling between the coating and the metal substrate is a significant character in the protection role of the CPs. Through this coupling the oxidized form of polymer (oxdPPy) shifts the metal substrate potential to positive direction and maintains the oxide surface of the substrate according to chemical equation (2). The reduction of oxygen may be involved the re-oxidation of the reduced form of polymer (redPPy) as indicated by the chemical equation (3). The comparison between the corrosion resistance behavior of the PPy coatings for Al in this study and that for stainless steel, in previous study [9], in acid solution indicates lower protection effect of the PPy coating for Al. This could be attributed to the lower galvanic coupling between the Al substrate and the PPy layer due to different nature of surface oxide film of Al and that of stainless steel.

$$\frac{1}{n} M + \frac{1}{m} oxdPPy + \frac{y}{n} H_2O \rightarrow \frac{1}{n} M(OH)_y^{(n-y)+} + \frac{1}{m} redPPy + \frac{y}{n} H^+ \tag{2}$$

$$\frac{1}{4} m\, O_2 + redPPy + \frac{1}{2} m\, H_2O \rightarrow oxdPPy + m\, OH^- \tag{3}$$
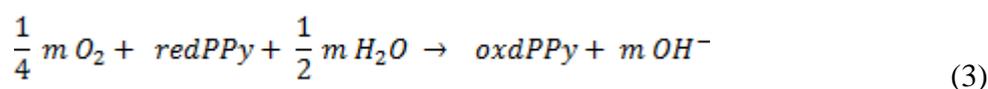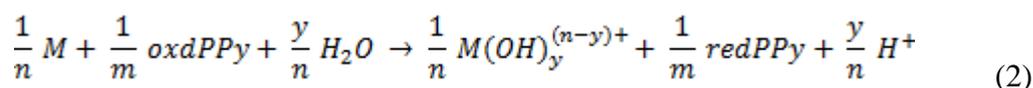
Figure 9 shows the potential-time behavior of the different coated Al samples in 0.1 M NaCl at room temperature. The bare of Al started with potential -0.825 V then it reached rapidly to a steady state potential ~ -0.930 V. All the polymer-coatings make the Al electrode at much noble potentials, and then it shifted rapidly to less noble in two stages of steady state potentials. The first stage was around - 0.65 V at which the coated Al potential remained temporary before decay again to less noble. Different values of the final steady potential for the different coated Al electrodes were obtained. The lowest steady state potential was exhibited by the neat PPy coating and which was about 100 mV nobler than that of the bare Al. The PPy-NiLa coated Al showed slightly positive shift in the second stage and exhibited highest positive final steady potential which is 250 mV more positive than that of the bare Al. This reflects good protection coating for Al substrate in the concentrated chloride solution.

The above results of the corrosion tests indicate improvements in the protection performance of the PPy coating by introducing the nanoparticles, more advance in case of the NiLa oxide particles particular in chloride solution. In our recent study, NiLa ferrite nanoparticles enhanced the coating properties of epoxy resin for stainless steel substrate [48]. It is suggested that these nanoparticles enhanced the coating character of the PPy through different ways. One way is improvement in the galvanic coupling by the catalytic effect of oxygen reduction and re-oxidation of the reduced state of the polymer (equation 3) [32]. Second way is a blocking effect of micro-pores in the polymer film. The more condensed layers of the polymers in presence of nanoparticles (composite films) may have less micro-pores in comparison with the neat PPy. And finally, the nanoparticles as adhesion promoters, the higher adhesion of the composites films than that of the neat PPy film indicates the adhesion promoter roles of the nano-particles, particularly of the Ni-La particles.

4. CONCLUSIONS

The addition of sCNTs and NiLa oxide nanoparticles to the aqueous electrolyte solution increased the electrodeposition rate of polypyrrole on the aluminum substrate. The influence of the

second addition of nanoparticles is larger on the deposition of the PPy. The additives enhanced the adhesion of the polymer films on the metal substrate. The sCNTs increased the thermal stability of PPy while the NiLa oxide nanoparticles decreased this stability. However, the PPy-NiLa nanocomposite provided higher significant improvement than the PPy-sCNTs nanocomposite in the corrosion resistance for the coated aluminum in acidic and chloride solution. Most likely, the NiLa oxide nanoparticles increased the barrier effect of the polymer layer, and they catalyzed the oxygen reduction reaction which enhances the passive state of aluminum.

References

1. Y. Yin, T. Liu, S. Chen, T. Liu, S. Cheng, *J. Appl. Surf. Sci.* 255 (2008) 2978.
2. O. Zubillaga, F.J. Cano, I. Azkarate, I.S. Molchan, G.E. Thompson, A.M. Cabral, P.J.Morais, *Surf. Coat. Technol.* 202 (2008) 5936.
3. J. Molina, A. Zille, J. Fernández, A.P. Souto, J. Bonastre, F. Cases, *Synth. Met.,* 204, (2015)110.
4. 4- A. A. Hermas, Z. X. Wu, M. Nakayama, and K. Ogura, *J. Electrochem. Soc.* 153 (2006) B199.
5. A.A. Hermas, *Prog. Org. Coat.* **61** (2008) 95.
6. G.B. Street, Handbook of Conducting Polymers, Marcel Dekker, New York, 1986, 265 p.
7. M. Saremi', M. Yeganeh, *Corr. Sci.* 86 (2014) 159.
8. I.L. Lehr, O.V. Quinzani, S.B. Saidman, *Mater. Chem. and Phys.* 117 (2009) 250.
9. A.A. Hermas, M. Nakayama, K. Ogura, *Electrochim. Acta*, 50 (2005) 3640.
10. S. Biallozor, A. Kupniewska, *Synth. Met.* 155 (2005) 443.
11. Zoran Grubaˇc, Ivana ˇSkugor Ronˇcevi ´c, Mirjana Metikoˇs-Hukovi ´c, *Corr. Sci.*, 102 (2016) 310.
12. Maocheng Yan , Christopher A. Vetter, Victoria J. Gelling, *Corr. Sci.* 70 (2013) 37.
13. S.T. Earley, D.P. Dowling, J.P. Lowry, C.B. Breslin, *Synth. Met.* 148 (2005) 111.
14. W.J. Hamer, L. Koene, J.H.W. de Wit, *Mater. Corr.* 55 (2004) 653.
15. D.E. Tallman, G. Spinks, A. Dominis, et al., *J. Solid State Electrochem.* 6 (2002) 73.
16. C.B. Breslin, A.M. Fenelon, K.G. Conroy, *Mater. Des.* 26 (2005) 233.
17. P. Hülser, F. Beck, *J. Appl. Electrochem.* 20 (1990) 596.
18. K.R.L.Castagnoa, Viviane Dalmorob, Denise S. Azambujab, *Mater. Chem. and Phys.* 130 (2011) 721.
19. B.D. Mert, R.Solmaz, G.Kardas, B.Yazıcı, *Prog. Org.c Coat.* 72 (2011) 748.
20. Metehan C. Turhan, M. Weiser, H. Jha, S. Virtanen, *Electrochim. Acta* 56 (2011) 5347.
21. Y. Chen, G. Kang, H. Xu, L. Kang, *Synth. Met.,* 215 (2016) 50.
22. F.G. Torres, O.H. Arroyo, C. Gomez, *J. Thermoplast. Compos. Mater.* 20 (2007) 207.
23. M. Merisalu, T. Kahro, J. Kozlova, A. Niilisk, A. Nikolajev, M. Marandi, A. Floren, H. Alles, V. Sammelselg, *Synth. Met.,* 200 (2015) 16.
24. H. Cong, J. Zhang, M. Radosz, Y. Shen, *J. Membr. Sci.* 294 (2007) 178.
25. D. Schmidt, D. Shah, E.P. Giannelis, Curr. Opinion *Solid State Mater. Sci.* 6 (2006) 205.
26. Başak Doğru Mert, *Corr. Sci.* 103 (2016) 88.

27. L. Iglesias-Rubiane, S.J. Garcia-Vergara, P. Skeldon, G.E. Thompson, J. Ferguson, M.Beneke, *Electrochim. Acta* 52 (2007) 7148.
28. A. Bhattacharya, K.M. Ganguly, A. De, S. Sarkar, *Mater. Res. Bull*. 31 (1996) 527.
29. Y. Zhu, J.O. Iroh, *J. Adv. Mater*. 34 (4) (2002) 16.
30. D.M. Lenz, C.A. Ferreira, M. Delamar, *Synth. Met*. 126 (2002) 179.
31. A.A. Hermas1, S.S. Al-Juaid, S.A. Al-Thabaiti, A.H. Qusti, M. Abdel Salam *Prog. Org. Coat.* 75 (2012) 404.
32. M. Abdel Salam, S.S. Al-Juaid**,** A.H. Qusti**,** A.A. Hermas, *Synth. Met.* 161 (2011) 153.
33. M.S.Abdel-Aal, M.TH.Makhlof and A.A.Hermas, *Brit. Corr. J.* 30 (1995) 70.
34. B.M. Abu-Zied, A.M. Asiri, *J. Nanomater.* 2012 (2012) 1.
35. M.A. Lucio Garcıa, Mascha A. Smit, *J. Power Sources* 158 (2006) 397.
36. T. Tuken, *Surf. Coat. Technol*. 200 (2006) 4713.
37. M.B. Gonzalez, S.B. Saidman, *Corr. Sci.* 53 (2011) 276.
38. A.A. Hermas, S.S. Al-Juaid, S.A. Al-Thabaiti, A.H. Qusti, M. Abdel Salam, *Prog. Org. Coat*. 75 (2012) 404.
39. P. Mavinakuli, S. Wei, Q. Wang, A.B. Karki, S. Dhage, Z. Wang, D.P. Young, Z. Guo, *J. Phys. Chem*. C 114 (2010) 3874.
40. T. Sandu, A. Sårbu, F. Constantin, C.I. Spătaru, R.A. Gabor, R. Şomoghi, H. Iovu, *Rev. Roum. Chim*. 57 (2012) 177.
41. P.S. Abthagir, R. Saraswathi, Thermal stability of polypyrrole prepared from a ternary eutectic melt, *Mater. Chem. and Phys*. 92 (2005) 21.
42. B. Zhang, Y. Xu, Y. Zheng, L. Dai, M. Zhang, J. Yang, Y. Chen, X. Chen, J. Zhou, *Nanoscale Res. Lett.* 6 (2011) 431.
43. N.G. Sahoo, Y.C. Jung, H.H. So, J.W. Cho, *Synth. Met*. 157 (2007) 374.
44. Lapides I, Borisover M, Yariv S. J. *Thermal Anal. Calorimetry* 2011;105:921–929.
45. Lapides I, Borisover M, Yariv S. *J. Thermal Anal. Calorimetry* 2011;105:39–51.
46. A.M. Asiri, M.A. Hussein, B.M. Abu-Zied, A.-E.A. Hermas, *Composites: Part B* 51 (2013) 11–18.
47. Z. Guo, K. Shin, A.B. Karki, D.P. Young, H.T. Hahn, *J. Nanopart. Res*. 11 (2009) 1441.
48. A. M. Asiri, M. A. Hussein, B. M. Abu-Zied, A. A. Hermas *Polym. Compos.* 36 (2015) 1875.